

# We are IntechOpen, the world's leading publisher of Open Access books Built by scientists, for scientists

6,900

Open access books available

185,000

International authors and editors

200M

Downloads

Our authors are among the

154

Countries delivered to

TOP 1%

most cited scientists

12.2%

Contributors from top 500 universities



WEB OF SCIENCE™

Selection of our books indexed in the Book Citation Index  
in Web of Science™ Core Collection (BKCI)

Interested in publishing with us?  
Contact [book.department@intechopen.com](mailto:book.department@intechopen.com)

Numbers displayed above are based on latest data collected.  
For more information visit [www.intechopen.com](http://www.intechopen.com)



# Compact Coplanar Waveguide Metamaterial-Inspired Lines and Its Use in Highly Selective and Tunable Bandpass Filters

Alejandro L. Borja<sup>1</sup>, James R. Kelly<sup>2</sup>, Angel Belenguer<sup>1</sup>,  
Joaquin Cascon<sup>1</sup> and Vicente E. Boria<sup>3</sup>

<sup>1</sup>*Departamento de Ingeniería Eléctrica, Electrónica, Automática y Comunicaciones,  
Escuela, Politécnica de Cuenca, Universidad de Castilla-La Mancha*

<sup>2</sup>*School of Electronic, Electrical and Computer Engineering, University of Birmingham*

<sup>3</sup>*Instituto de Telecomunicaciones y Aplicaciones Multimedia,  
Universidad Politécnica de Valencia*

<sup>1,3</sup>Spain

<sup>2</sup>UK

## 1. Introduction

During the last years, the metamaterials field has grown rapidly due to the possibility of accomplishing a methodology to achieve negative effective parameters  $\epsilon_{eff}$  Pendry et al. (1996) and  $\mu_{eff}$  Pendry et al. (1999), and their experimental verification Smith et al. (2000) - Shelby, Smith & Schultz (2001). The main research work has been concentrated on the theoretical consequences of negative parameters, as well as techniques for practically realizing left-handed media for various optical/microwave concepts and applications. Among recent concepts, properties, and devices based on engineered metamaterials, we can mention frequency selective structures, which have opened the path to a new range of passive devices for guided applications. In this context, split ring resonator (SRR) loaded transmission lines represent the cutting edge of research in the field of one-dimensional (1D) planar left-handed structures. These structures were firstly proposed by Martin et al. in 2003 Martin et al. (2003) by magnetically coupling a shunted coplanar waveguide (CPW) and pairs of SRRs. These planar devices exhibit backward propagation in a narrow frequency band above the resonant frequency of the rings, with the necessary degree of flexibility to design compact low insertion losses filters. Thus, based on this former configuration different approaches have been proposed with the aim of improving performances and overcome possible drawbacks such as asymmetrical response shape or transmission bands with smooth edges. For instance, a combined right/left-handed CPW structure was implemented by cascading SRRs-wire and SRRs-gap stages Bonache et al. (2005), satisfactorily achieving a transmission upper band with a sharp cut-off. Furthermore, new CPW lines with extra loading elements have shown interesting properties in terms of improved out-of-band behavior and response selectivity Borja, Carbonell, Boria, Cascon & Lippens (2010) - Borja, Carbonell, Boria &

Lippens (2010b). By these means, it is possible to control several restrictive trade-offs by simply adjusting the loading elements. In this way it is possible to obtain quite a symmetric frequency response along with controllable bandwidths and compact dimensions.

In this chapter, the properties of a variety of metamaterial designs are analyzed and discussed in order to develop novel small planar metamaterial frequency selective structures. The study of these configurations is based on full-wave electromagnetic analysis, equivalent circuit simulations and measured responses of different prototypes designed for microwave operation. In particular, section 2 presents different CPW lines based on a split ring resonator SRR technology and loaded with metallic strips and gaps. The properties of such structures can be controlled by properly designing or adding loading elements. In this regard, the use of shunt wires permits to control frequency selectivity by means of an engineering of the electric plasma frequency, providing deeper upper band rejection levels. On the other hand, the addition of series capacitances to previous unit cell implementations provides a transmission response which is almost symmetric while exhibiting a right-handed character along the pass band, contrary to conventional left-handed lines. In sections 3 and 4 enhanced out-of-band rejection properties and reconfigurable responses can be obtained by the use of cascaded and varactor loaded basic cells, respectively. Finally, the main conclusions of the chapter are outlined in section 5.

## **2. Split ring resonators based coplanar waveguide lines**

In this section, different arrangements corresponding to configurations of SRRs loaded CPW lines have been considered. Two loading elements, i.e. shunt strips, and series gaps have been successively included in the CPW line. These inclusions are much smaller than the electrical wavelength of the propagating wave. Therefore, effective medium considerations in the CPW and lumped equivalent circuit models have been used to understand and better explain the complex features of wave propagation inherent to these loaded lines. In this section numerical studies and experiments are also included.

### **2.1 Split ring resonators loaded coplanar waveguide with shunt strips**

The first model is based on the combination of SRRs and shunt wires within a host CPW line. This resonant structure has already been deeply analyzed Martin et al. (2003), and therefore it will be used as a reference result. In summary, this unit cell behaves as a left-handed propagation uni-dimensional transmission line that, if its size is sufficiently small as compared to the electrical wavelength, can have a double negative effective medium behaviour. By using the SRRs it is possible to synthesize a negative value of effective permeability, whereas shunt wires in the CPW provide a negative effective permittivity. For this reason, the structure can be considered as a double negative effective medium, when operating at frequencies slightly above the resonance of the isolated SRR Aznar et al. (2008).

The proposed left-handed structure is depicted in Fig. 1. It consists of a host CPW loaded with SRRs and two shunt strips. SRRs are symmetrically placed on the rear of the substrate, while thin metal wires connect the signal line to the ground plane at positions coincident with the center of the SRRs. Table 1 defines the CPW geometry, unit cell characteristics, and common parameter values for this and subsequent configurations.

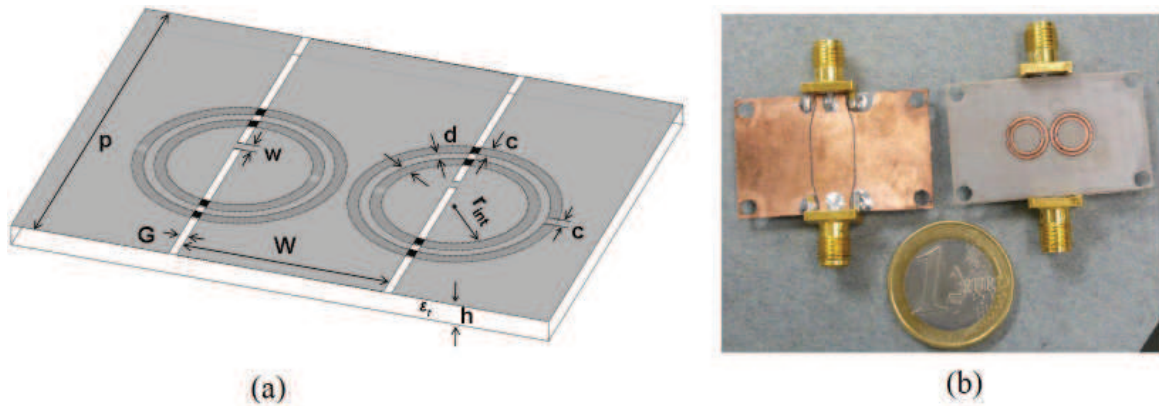


Fig. 1. (a) SRRs loaded CPW with shunt strips, and (b) photograph of the prototype.

$W(\text{mm})$	$G(\text{mm})$	$p(\text{mm})$	$w(\text{mm})$	$h(\text{mm})$	$\epsilon_r$
7.7	0.3	10	0.4	0.508	2.2
$\text{tg}\delta$	$t(\mu\text{m})$	$\sigma(\text{S/m})$	$r_{int}(\text{mm})$	$c(\text{mm})$	$d(\text{mm})$
0.0009	35	$5.8 \cdot 10^7$	2.6	0.4	0.4

Table 1. Unit cell characteristics.

$W$  is the line width,  $G$  is the gap between conductors,  $w$  is the strip width, and  $p$  the unit cell period. Substrate characteristics are height  $h$ , permittivity  $\epsilon_r$ , and loss tangent  $\text{tg}\delta$ . Copper metallization was utilized. This had a thickness  $t$ , and conductivity  $\sigma$ . Moreover, a prototype has been fabricated in order to verify the propagation behavior of the cell, see Fig. 1 (b). A taper section is added at both SMA connections to properly feed the device. The sample has been fabricated on a Neltec NY9220 dielectric substrate using a mechanical milling process. The milling was performed by a LPKF Protomat 93S machine. Thereafter, the fabricated device has been measured and characterized by means of a Rohde & Schwarz vector network analyzer ZVA-24, calibrated with a Through-Open-Short-Match kit, in the frequency band from 3 to 5 GHz.

In parallel, the structure proposed is analyzed and compared with the lumped element equivalent circuit of the unit cell, see Fig. 2. Due to physical symmetry properties, the magnetic wall concept has been used so that the equivalent circuit corresponds to one half of the basic cell. The equivalent circuit model can be transformed to an equivalent  $\pi$ -circuit type, as it was described by Aznar et al. (2008),

Each SRR can be represented by a simple LC parallel resonator circuit in the vicinity of resonance, with elements  $L_s$  and  $C_s$ .  $L$  and  $C$  are the per-section inductance and capacitance defined from the geometry of the CPW line and calculated as it is advised in Mongia et al. (1999).  $L_p$  is the equivalent inductance of connecting wires, which divides the inductances  $L_s$  and  $L$  into two parts, as proposed in Rogla et al. (2007) and thoroughly verified in Aznar et al. (2008). SRRs are modeled by parallel resonant circuits inductively coupled to the line through a coupling constant  $k$ . It is calculated by means of the fractional area theory explained in Martin et al. (2003). The values of the different lumped elements and parameters are summarized in Table 2.

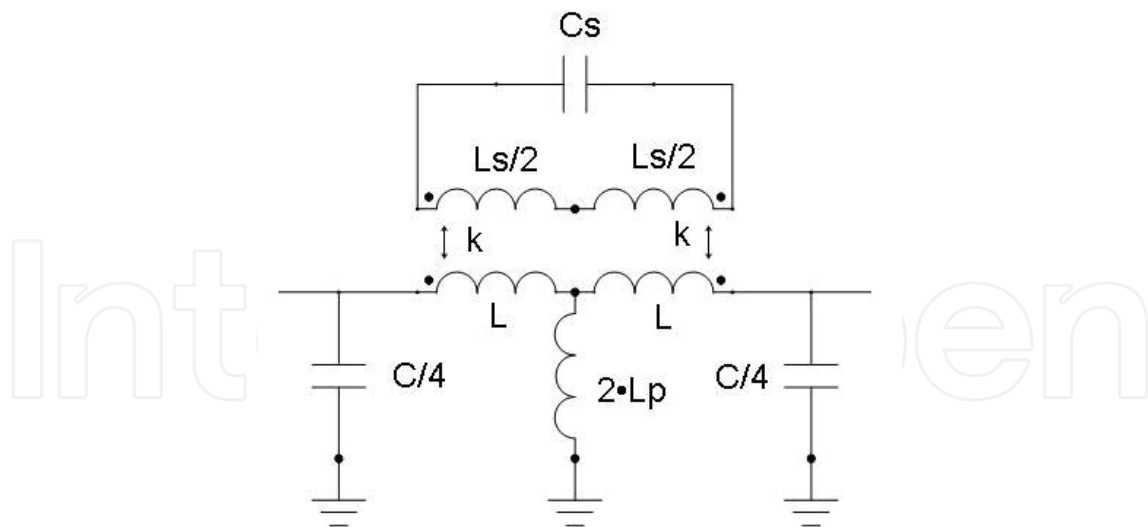


Fig. 2. Lumped equivalent circuit model of the SRRs loaded CPW with shunt strips, originally proposed in Rogla et al. (2007).

$C_s$ (pF)	$L_s$ (nH)	$C$ (pF)	$L$ (nH)	$L_p$ (pH)	$k$
0.104	14.8	0.672	2.11	131	0.342

Table 2. Equivalent circuit parameters of the SRRs loaded CPW with shunt strips.

The transmission  $S_{21}$  and reflection  $S_{11}$  coefficients for the left-handed structure shown in Fig. 3 (a), have been obtained from three different sources, i. e. full-wave simulations, lumped equivalent circuit simulations, and experimental results. Agreement is found to be very good in all cases. Nonetheless, a frequency shift for the equivalent circuit response is observed. This shift could be minimized by simply tuning  $L_s$  and  $C_s$  element values, which control the SRR resonance. As it can be seen, the frequency response exhibits a pass band centred around 4.3 GHz with a transmission zero close to 3.6 GHz. According to the model of Fig. 2, the structure should exhibit a transmission zero (all injected power is returned back to the source) at that frequency where the series branch opens, and it occurs at the resonant frequency of the coupled SRRs.

The analysis of these transmission characteristics is performed by the extraction of the effective medium parameters of the uni-dimensional propagation structure, see Fig. 3 (b). The extraction is based on the well known Nicolson-Ross-Weir (NRW) procedure used in Smith et al. (2005), where the real parts of the permittivity and permeability are retrieved from the scattering parameters. The results obtained confirm the presence of a narrow pass band between 4.1 GHz and 4.5 GHz, corresponding to a double negative frequency band as it is expected. The maximum transmission is achieved when the matching condition  $\epsilon \cong \mu$ , and thus reduced impedance  $\bar{Z} = \sqrt{\mu/\epsilon} \cong 1$ , is satisfied. Henceforward, the transmission line becomes single negative as permeability reaches positive values after the magnetic plasma frequency  $f_{mp}$ . A double positive medium is subsequently obtained above the electric plasma frequency  $f_{ep}$ .

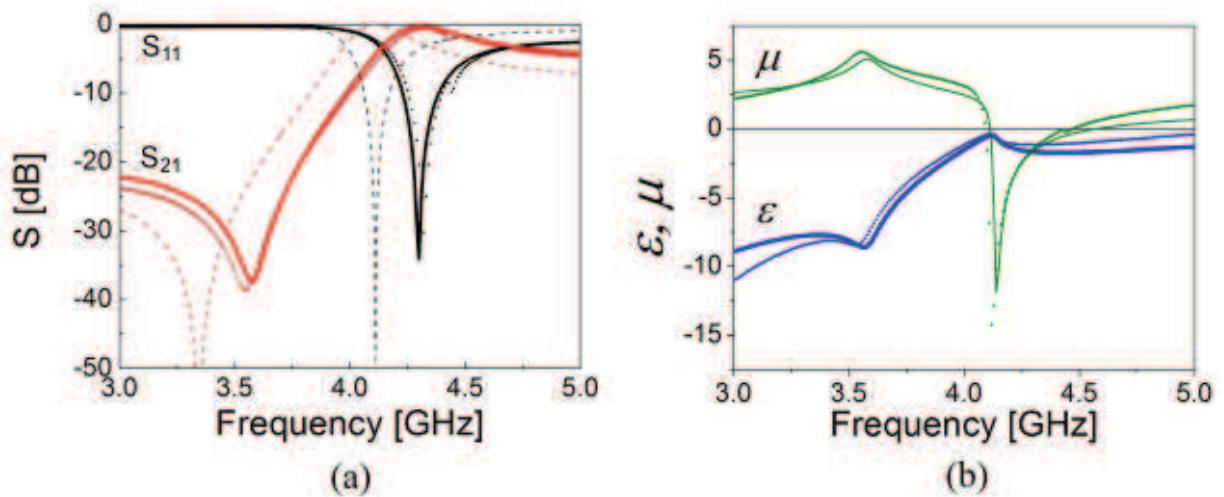


Fig. 3. (a) Simulated and experimental  $S_{11}$  and  $S_{21}$  parameters. (thick solid line: Full-wave simulation, symbol: Measurement, thin dashed line: lumped equivalent circuit simulation). (b) Simulated (line) and experimental (symbol) real parts of extracted permittivity (thick) and permeability (thin) according to the NRW method.

## 2.2 Split ring resonators loaded coplanar waveguide with series gaps

The next model, depicted in Fig. 4 (a), is based on the combination of SRRs and series gaps. In this configuration, the shunt wires located on the top side of the substrate have been substituted by series gaps. These elements are dual of the shunt wires and they are located symmetrically with regard to the center of the unit cell. The dimensions of the elements, defined in Table 1, are the same ones as those considered in the previous configuration. Moreover, the gap width  $g$  and separation  $p_1$  are 0.25 mm and 5 mm, respectively. A prototype has been manufactured in order to verify the behaviour experimentally, see Fig. 4 (b). The sample has been fabricated using the same substrate and process described in section 2.1.

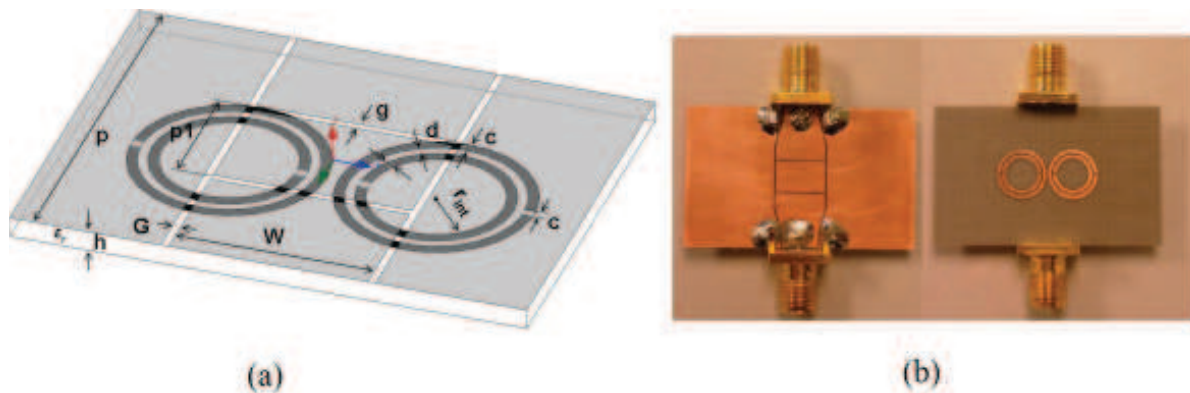


Fig. 4. (a) SRRs loaded CPW with series gaps and (b) photograph of the prototype.

Likewise, a lumped element equivalent circuit of the elemental cell, shown in Fig. 5, is used to assess the different properties of the new configuration under study. The CPW is modeled as described before, it includes two series capacitances which have been properly modified accordingly to the magnetic wall theory. A gap discontinuity in a CPW line can be represented by means of an equivalent two-port  $\pi$ -network, as presented by Deleniv et al. (1999). The

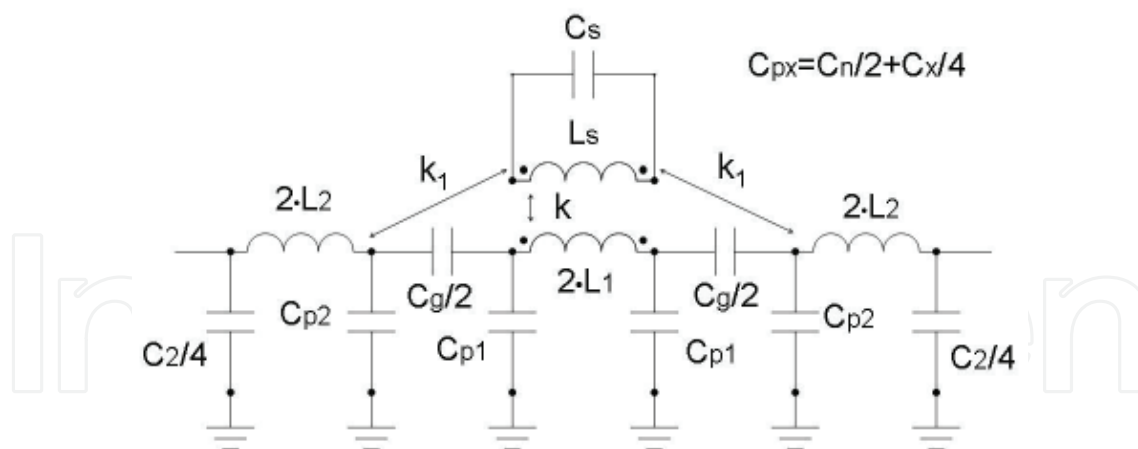


Fig. 5. Lumped equivalent circuit model of the SRRs loaded CPW with series gaps.

$\pi$ -network comprises a series capacitance  $C_g$  together with a shunt capacitance  $C_n$ . The series capacitance  $C_g$  describes the reactance due to the gap discontinuity, whilst the shunt capacitance  $C_n$  accounts for grounding edge effects at the sides of the gap.  $L_1$  and  $C_1$  are the per-section inductance and capacitance of the line between the gaps. Also,  $L_2$  and  $C_2$  account for the per-section inductance and capacitance of the transmission line.  $C_{pi}$  ( $i=1,2$ ) is the equivalent capacitance of the two shunt capacitances,  $C_{n/2}$  and  $C_{i/4}$ . The SRRs are inductively coupled to different parts of the line. Coupling to the central portion of the line, between gaps, is modeled by a coupling constant  $k$ .  $k$  is calculated applying the fractional area theory. The value of  $k$  has been adjusted slightly since the series gaps modify the coupling between the line and the rings. Following this adjustment, the bandwidth and location of the transmission zero can easily be tuned. Similarly, the coupling constant  $k_1$  represents the interaction between the external portions of the CPW and the SRRs. The value of  $k_1$  was adjusted by means of a curve fitting procedure, which ensured that the equivalent circuit simulations agreed well with the measurement results. Table 3 gives the final values of the circuit elements within the equivalent circuit.

$C_s$ (pF)	$C_g$ (pF)	$C_n$ (pF)	$C_1$ (pF)	$C_2$ (pF)
0.104	0.3	0.0485	0.3192	0.1596
$L_s$ (nH)	$L_1$ (nH)	$L_2$ (nH)	$k$	$k_1$
14.8	1	0.5	0.6	0.35

Table 3. Equivalent circuit parameters of the SRRs loaded CPW with series gaps.

Fig. 6 (a) shows the scattering parameters obtained through simulation and measurement. A good agreement between the three responses, i.e. full-wave, equivalent circuit, and measurements is observed. As a relevant feature, it can be mentioned that the structure exhibits a transmission band centred around 3.8 GHz and a transmission zero around 4.5 GHz. This is contrary to the performance of a CPW line loaded with SRRs and shunt strips, where the transmission zero is located below the pass band, see Fig. 3 (a). In this structure the transmission zero is located at high frequencies and the pass band appears before the anti-resonance. An important reminder here is that the SRRs are exactly the same in these two configurations, and only the other loading elements (series gaps and shunt wires, not resonant

by themselves in this frequency range) are different. The parallel inductive contribution of the wires is replaced by a series capacitance. For this reason the device exhibits dual behaviour compared to a CPW line loaded with SRRs and shunt strips.

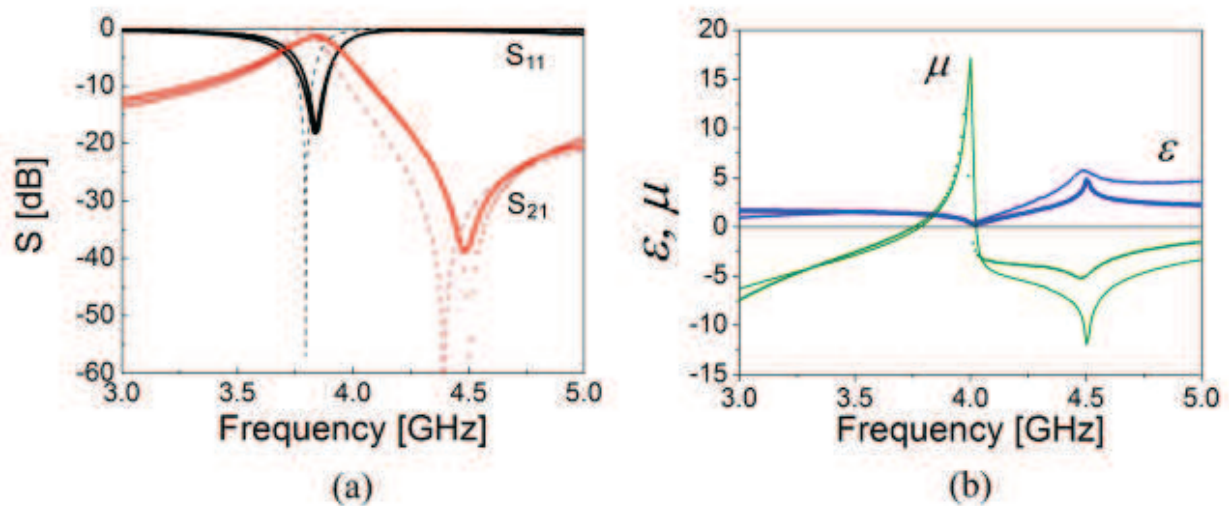


Fig. 6. (a) Simulated and experimental  $S_{11}$  and  $S_{21}$  parameters. (thick solid line: Full-wave simulation, symbol: Measurement, thin dashed line: lumped equivalent circuit simulation). (b) Simulated (line) and experimental (symbol) real parts of extracted permittivity (thick) and permeability (thin) according to the NRW method.

This performance can be explained by the interpretation of the retrieved permittivity and permeability of the structure, presented in Fig. 6 (b). The generation of a pass band is related to a double-positive condition. Permittivity remains positive in the whole measured frequency band. Permeability is also positive in a small frequency range, below the resonant frequency of the SRR (4 GHz), and negative with a monotonous variation outside it. In this case, the SRR is contributing to generate a right-handed transmission band. This is due to the series capacitance loaded in the line, which precludes transmission outside of the area where the SRR resonates. Permittivity is also affected by the presence of the SRR, but it remains positive as mentioned before. Note also, as expected, that peak transmissions correspond to the different crossings of the  $\epsilon$  and  $\mu$  curves ( $\epsilon \cong \mu$  gives the matching condition and hence maximum transmission and minimum reflection). The transmission zero in Fig. 6 (b) is located coincident with the positions of the slope changes in the effective parameters. These slope changes are in turn due to the superposition of the 'monotonous' behaviours of the simple loading elements (series gaps) with the complex (quasi-Lorentz-type) behaviour of the SRR loaded in the line.

### 2.3 Split ring resonators loaded coplanar waveguide with shunt strips and series gaps

At last, the characteristics of transmission lines combining all the previous elements, shunt strips and series gaps in CPW technology are studied. The unit cell, described in Fig. 7 (a), consists of an SRRs based CPW loaded with two shunt metallic strips and two series capacitances.

The gaps are symmetrically placed with respect to the SRRs, while the thin shunt strips connecting the central line to the ground are placed at those positions coincident with the

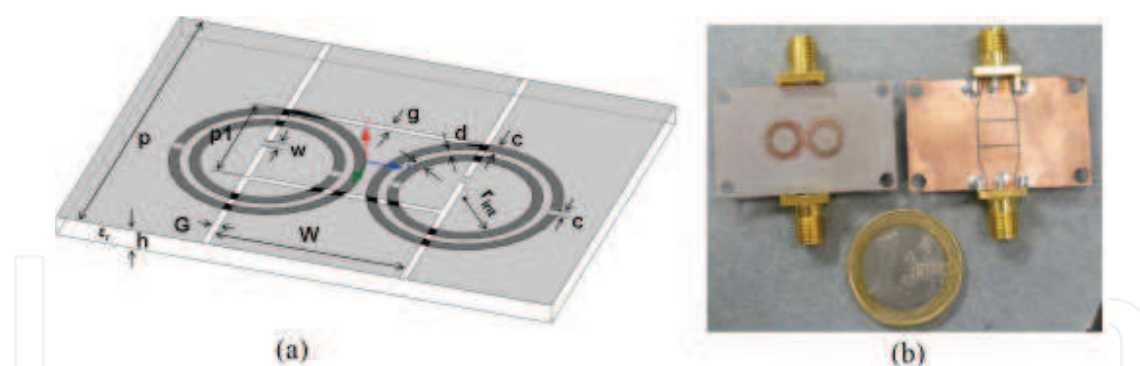


Fig. 7. (a) SRRs loaded CPW with shunt strips and series gaps, and (b) photograph of the prototype.

center of the SRRs. The series gap elements can be interpreted as the dual counterpart of the shunted inductive strips as it was discussed previously. These elements, shunt strips and series gaps, are in the coupling regions of the SRRs so that, as it is next explained, combined effects of previous properties take place. The configuration of the unit cell is the same as that employed in previous sections. The dimensions are given in Table 1. In Fig. 7 (b), the prototype of the unit cell is depicted.

The lumped equivalent circuit model of the basic cell, which will be used for the interpretation of the structure, is presented in Fig. 8. As it was reported previously, due to symmetry, the magnetic wall theory has been applied. In addition, the different elements of the circuit model are identical to those described in sections 2.1 and 2.2 (see also Table 4).

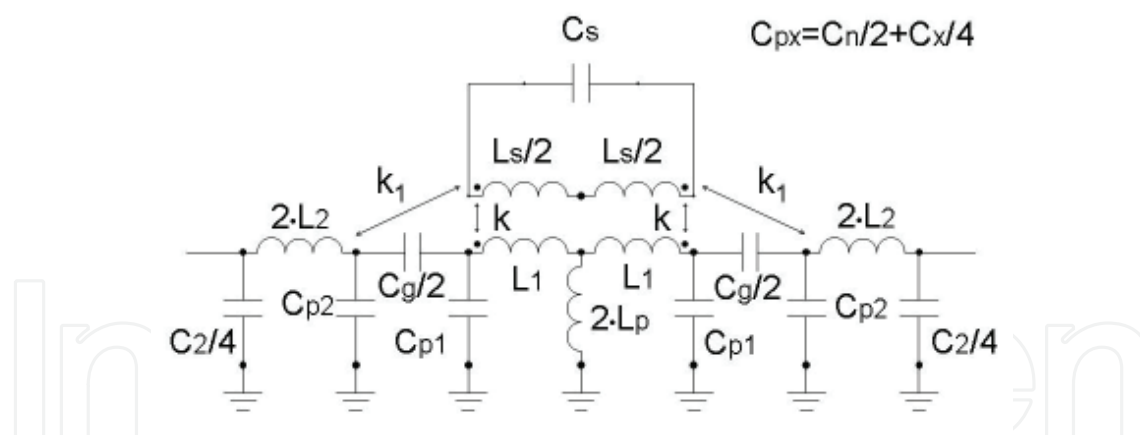


Fig. 8. Lumped equivalent circuit model of the SRRs loaded CPW with shunt strips and series gaps.

$C_s$ (pF)	$C_g$ (pF)	$C_n$ (pF)	$C_1$ (pF)	$C_2$ (pF)	
0.104	0.44	0.0485	0.588	1.3	
$L_s$ (nH)	$L_1$ (nH)	$L_2$ (nH)	$L_p$ (pH)	$k$	$k_1$
14.8	1.84	4.08	131	0.6	0.1

Table 4. Equivalent circuit parameters of the SRRs loaded CPW with shunt strips and series gaps.

The simulated and measured frequency responses for the proposed structure are shown in Fig. 9 (a). An excellent agreement between full-wave simulation data and experimental results can be observed. There is also satisfactory agreement between the results obtained using the proposed equivalent circuit and those derived by other means.

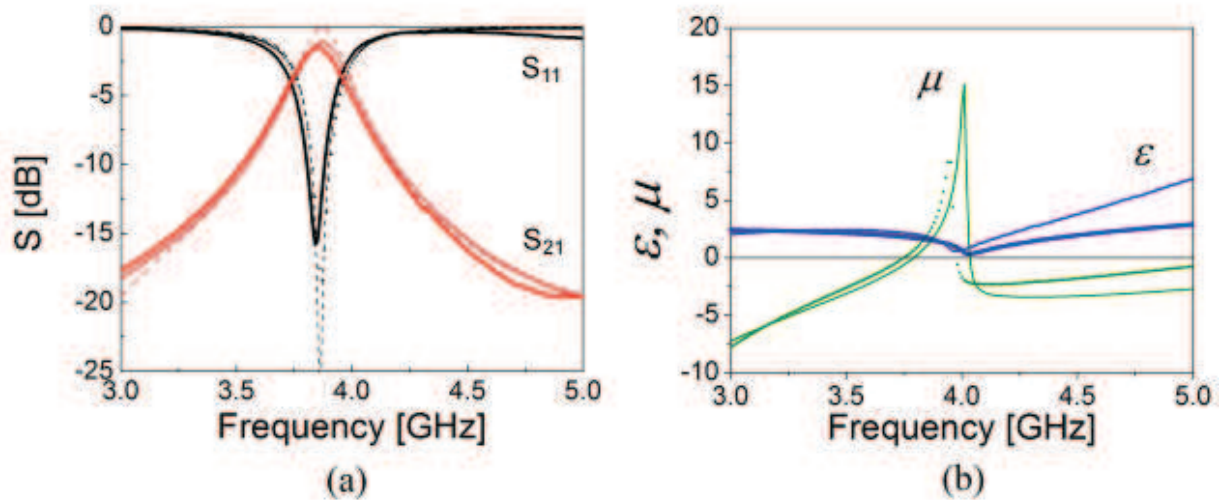


Fig. 9. (a) Simulated and experimental  $S_{11}$  and  $S_{21}$  parameters. (thick solid line: Full-wave simulation, symbol: Measurement, thin dashed line: lumped equivalent circuit simulation). (b) Simulated (line) and experimental (symbol) real parts of extracted permittivity (thick) and permeability (thin) according to the NRW method.

In the two cases previously studied, namely SRR loaded CPW with shunt strips and SRR loaded CPW with series gaps, a highly asymmetric frequency response with a characteristic anti-resonance effect (dip in the transmission) was obtained. In contrast, the frequency dependence of the cell with strips and gaps simultaneously exhibits an almost symmetrical pass band response centred around 3.9 GHz, just below the intrinsic SRR resonance. There are no transmission zeros in the vicinity of this pass band.

The third structure exhibits better selectivity than the previous ones, where it was only improved at frequencies above the pass band. The absence of transmission zeros is attributed to the transmission levels of each single element. In a CPW line loaded by SRRs, the shunt strips generate a transmission zero at lower frequencies but permit transmission above pass band. For this reason, the transmission zero introduced by the gaps disappears. In the same way, the transmission zero introduced by the strips is cancelled by the high transmission levels due to the series gaps.

The pass band is associated with the double positive condition (positive permittivity and permeability), see Fig. 9 (b). This condition is only achieved over a very narrow range of frequencies around, 3.9 GHz. The absence of transmission zeros can be attributed to the lack of slope changes in the effective parameters. For the models studied in sections 2.1 and 2.2, the transmission zeros in Fig. 3 and Fig. 6 are located coincident with the position of the slope changes in the effective parameters. These slope changes are due to a superposition of effects caused by the simple loading elements (series gaps and shunt wires) and the SRR. In common with the CPW line loaded with SRRs and gaps, this structure has a right-handed behaviour.

For this reason one can conclude that the gaps effect would dominate over that of the shunt strips. Whenever shunt strips are used there will be a transmission zero in the lower part of the frequency spectrum. This is the only effect using shunt strips. The frequency response will be symmetric and right-handed if the gaps are present. Additionally, as it can be expected, peak transmission corresponds to the matched condition  $\epsilon \cong \mu$ .

### 3. Compact and highly selective left-handed transmissions lines loaded with split ring resonators and wide strips

In the present section, it will be shown numerically and experimentally that problems related to out-of-band rejection can be alleviated by a proper arrangement of the loading elements responsible of the electrical response (shunt wires). Also, it is demonstrated that the selectivity of the transmission window can be improved by cascading basic cells. This opens up the possibility to fabricate band pass filters based on the SRR technology with excellent trade-offs between selectivity, insertion losses, and out-of-band rejection.

#### 3.1 Split ring resonators loaded coplanar waveguide with wide shunt strips

The electromagnetic properties of left-handed materials, which are highly dispersive due to the transition between the single negative and double negative conditions, have shown interesting frequency filtering properties. These properties rely on the same physical principle, namely the magnetic coupling of a transmission medium to micro-resonators. This effect is responsible for producing a negative effective permeability above the resonant frequency of the resonators. On the other hand, an arrangement of shunt strips create a medium which exhibits negative values of the effective permittivity ( $\epsilon_{eff}$ ) and a high pass filter response. The overlap of the spectrum where  $\epsilon_{eff}$  and  $\mu_{eff}$  are simultaneously negative gives a frequency band in which the wave propagation is backward. This correspond to the so-called Left-Handed (LH) rule in terms of  $E$ ,  $H$  and  $k$  trihedron. Indeed, it is now well established that the dispersion properties of the negative effective permittivity and permeability are very different, with a Drude-like and Lorentz-type frequency variation, respectively (see Fig. 10).

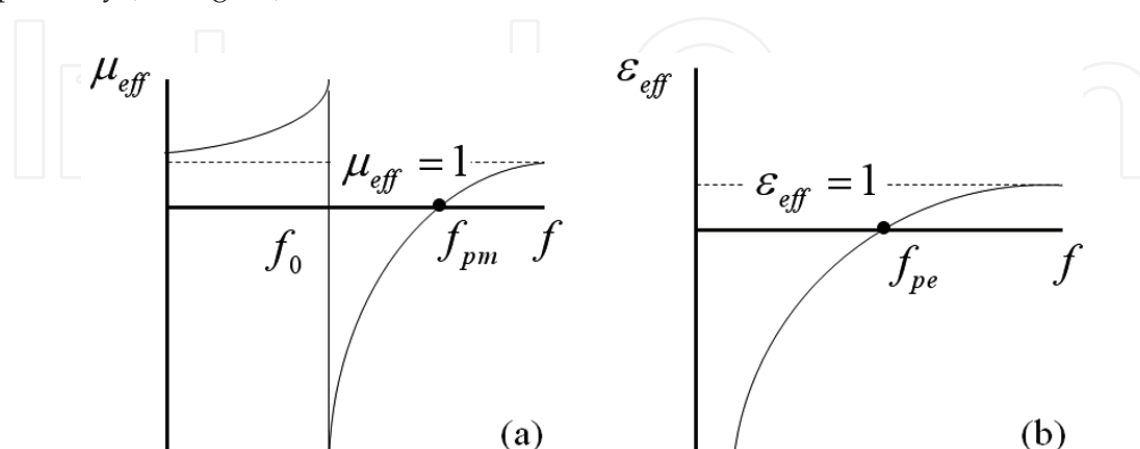


Fig. 10. (a) Lorentz-type model and (b) Drude-like model.

In short, whereas the permittivity increases continuously from negative values to positive ones, at the crossing point known as the electrical plasma frequency, the variations of the effective permeability versus frequency show a resonant response. The two frequencies involved are the resonance frequency of resonators and the magnetic plasma frequency. As a consequence, the asymmetric and double negative overall response is the superposition of a resonant transmission onto a baseline that increases with frequency. Under these conditions, the electrical plasma frequency which defines the transition between the negative and positive value of  $\epsilon_{eff}$  is generally adjusted until it is slightly higher than the magnetic plasma frequency. By this choice it is generally believed that the impedance matching conditions can be met with comparable values of  $\mu$  and  $\epsilon$  and hence impedance  $Z \approx 1$ .

An alternative technique for improving the selectivity of the transmission window is proposed below, without any additional loading elements. It is based on the engineering of the electric plasma frequency  $f_{pe}$ . The idea is to increase  $f_{pe}$  with respect to the magnetic plasma frequency  $f_{pm}$ . In this way it is possible to ensure that the material is single negative over a broader range of frequencies. Consequently, the rejection level is increased in the upper part of the spectrum. In addition, the impedance matching conditions are not significantly degraded due to the fact that the effective permittivity is also influenced by the resonance effect of the SRRs. For this reason, the values of  $\epsilon_{eff}$  are still quite comparable to those of  $\mu_{eff}$  in the vicinity of the resonance.  $f_{pe}$  is tailored by enlarging the width of the shunt strip. This also has the effect of dramatically decreasing the coupling between the resonator and the CPW line. As a consequence, the selectivity of the left-handed pass band is enhanced. The model proposed in section 2.1 is further analyzed in order to improve its frequency response. Fig. 11 (a) shows a general schematic of the unit cell.

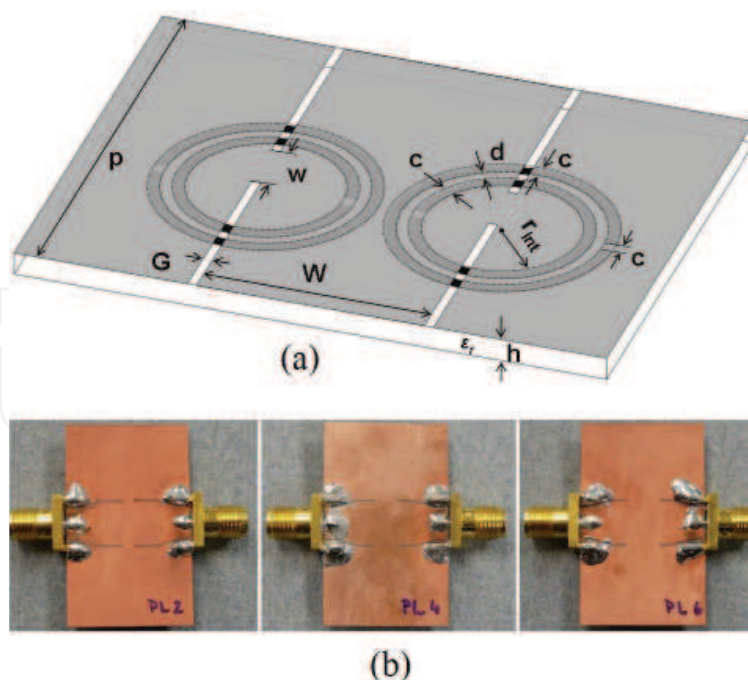


Fig. 11. (a) SRRs loaded CPW with wide shunt strips configuration, and (b) photograph of prototypes with widths  $w=2, 4$  and  $6$  mm, respectively.

The dimensions and characteristics are given in Table 1. Additionally, Fig. 11 (b) shows three fabricated prototypes with identical dimensions, only  $w$  has been modified for the different devices. The width of connecting wires is varied from  $w=2$  mm to  $w=6$  mm, in 2 mm steps. In previous implementations,  $w$  was approximately equal to the SRR strip width  $c$  (where  $c=0.4$  mm). In this case,  $w$  was increased by a factor of 10. With these SRR dimensions, the unloaded  $Q$  factor calculated using the eigenmode solver in HFSS, was found around 400. This assumes a copper conductivity of  $\sigma = 5.8 \cdot 10^7$  S/m and dielectric loss tangent of  $\text{tg } \delta=0.0009$ . Next, the simulated and measured responses are compared. Fig. 12 shows the scattering parameters  $S_{11}$  and  $S_{21}$  as a function of frequency for the four single-cell prototypes, which simply differ by the width of the shunt strip  $w$  as aforementioned.

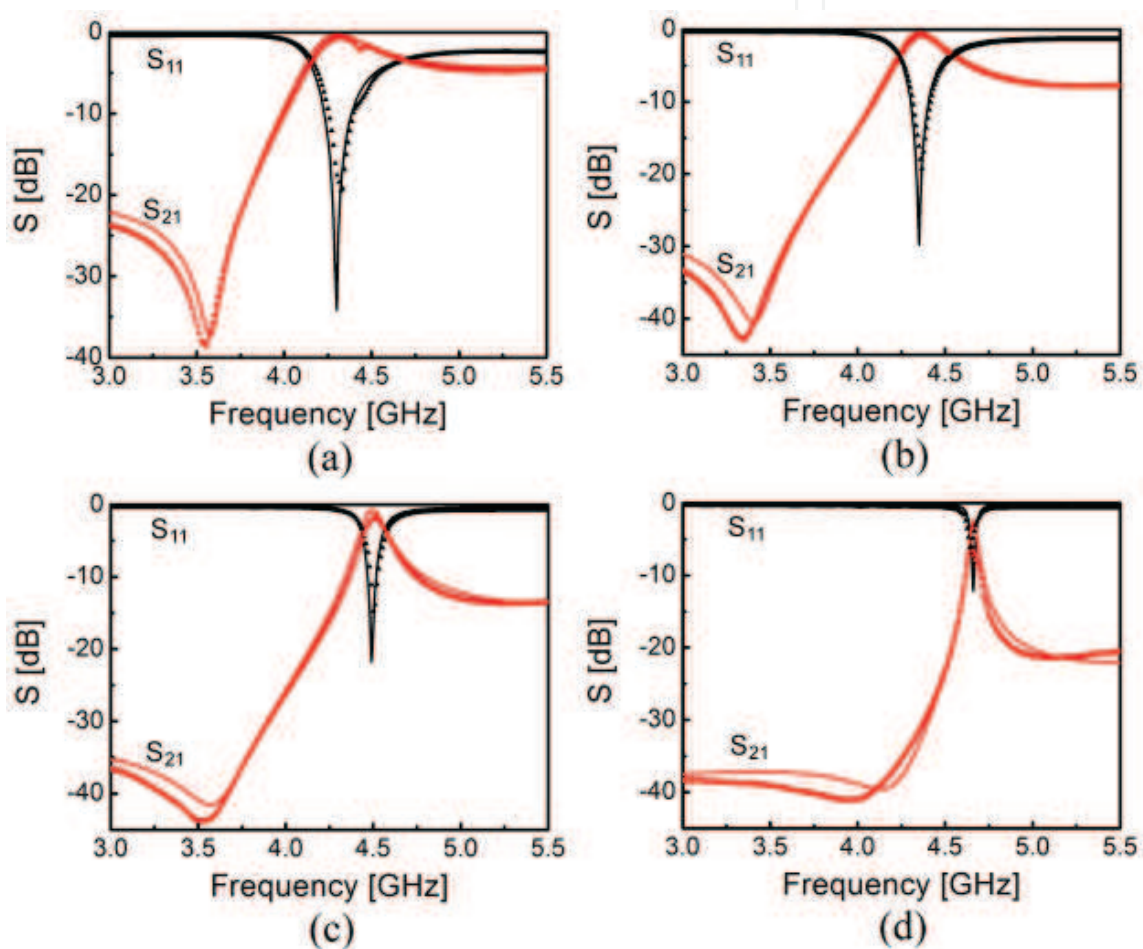


Fig. 12. Comparison between measured (symbol) and calculated (solid lines) scattering parameters for (a)  $w=0.4$  mm, (b)  $w=2$  mm, (c)  $w=4$  mm and (d)  $w=6$  mm.

In Fig. 12 (a) the width was set to  $w=0.4$  mm, while in Fig. 12 (b), (c), and (d) it was increased to  $w=2$  mm,  $w=4$  mm, and  $w=6$  mm respectively. In practice, the  $S_{ij}$  parameters were measured by means of a Vector Network Analyzer between 3 and 5.5 GHz. The calibration procedure is based on a Through-Open-Short-Match method. The tapered sections which interconnect the coaxial connector and the basic cell have been removed by a de-embedding process. Comparing Fig. 12 (a), (b), (c), and (d), it can be seen that enlarging the strip width by one order of magnitude, keeping the SRR geometry unchanged, has different major consequences:

an increase of the selectivity, a decrease of the bandwidth, a shift of the resonant frequency, and an increase of the insertion losses.

First of all, it can be noticed that the out-of-band rejection maximum at around 5 GHz which corresponds to the transmission level where the derivative of  $S_{21}$  is vanishing, shows a huge increase. Rejection levels are shown in Table 5. Let us keep in mind that such a high rejection level was obtained with a single cell. The measured return losses are equal to -20 dB for  $w=0.4$  mm at around 4.25 GHz, while they reach -15 dB for  $w=4$  mm at around 4.5 GHz, showing that the mismatch degradation is moderate, and compatible with real life applications where return loss around -10 dB can be enough.

	$w=0.4$ mm	$w=2$ mm	$w=4$ mm	$w=6$ mm
Out-of-band rejection (dB) at 5 GHz	-4.5	-7.6	-13	-22.7
FBW (%)	12.7	7.2	3.3	1.2

Table 5. Shunt strip effect on the out-of-band rejection and FBW.

Furthermore, it can be shown that the bandwidth at half maximum of the transmission is considerably narrower with a fractional bandwidth (FBW) decreasing from  $FBW = 12.7\%$  for  $w=0.4$  mm to  $FBW = 1.2\%$  for  $w=6$  mm, see Table 5.

Despite the fact that the SRR dimensions were kept unchanged between the four prototypes, a slight shift in the resonance frequency was observed. It is not due to fabrication tolerances, owing to the good fit with the full-wave simulation results. This shift is attributed to a slight alteration of the SRRs excitation, as a consequence of the modification of the strip. The interaction between SRRs and shunt strips is what determines in practice the position of the maximum transmission peak in the left-handed transmission band. Thus, as long as the width  $w$  is varied, the transmission band is shifted. Finally, it can be noted that there is a moderate increase in the insertion losses due to the increase in width of the shunt strip. It is for the reason that very selective frequency responses are deeply affected by the conductor and dielectric losses. Also, SRRs are weakly excited.

In order to have further insight into the electromagnetic properties in terms of dispersion characteristics, the frequency dependence of the effective parameters has been retrieved. To this aim, the Nicolson-Ross-Weir procedure, which has also been applied in section 2, is used. It is worthwhile to mention that the retrieval process is usually utilized when the dimensions of the unit cell are electrically small compared to the wavelength, generally  $\lambda_g/10$ . It means that when the working frequency increases the extracted parameters are less accurate. The applicability of such methods are strongly related to the frequency range where the device is considered to be used. Therefore, the results extracted from this analysis method should be considered as an estimation rather than an exhaustive study.

Fig. 13 shows the frequency dependence of the real parts of the effective permittivity and permeability for  $w=0.4$  mm and  $w=4$  mm. For simplicity, two values are shown, being enough to verify the effect of the shunt strip width increase. The key result is the observation of a shift of the frequency when  $\epsilon_{eff}$  goes from the negative values to positive ones, this corner frequency corresponding to  $f_{pe}$ . Quantitatively it can be seen that  $f_{pe}$  is shifted from 6.6 GHz to 8.8 GHz for simulations, and from 5.2 GHz to 7.4 GHz for measurements, when the strip width

is widened by an order of magnitude starting from  $w=0.4$  mm. It is also important to note that a resonant feature is superimposed on the conventional Drude-like variation ( $\epsilon = 1 - (\omega_{pe}/\omega)^2$ ) envelope, helping to keep good input impedances.  $\epsilon_{eff}$  reaches values comparable to the values of  $\mu_{eff}$  due to the resonant effect of the SRRs, thus having in both cases good impedance matching levels. On the contrary, the dispersion of the effective permeability is less affected by the increase of the strip width.

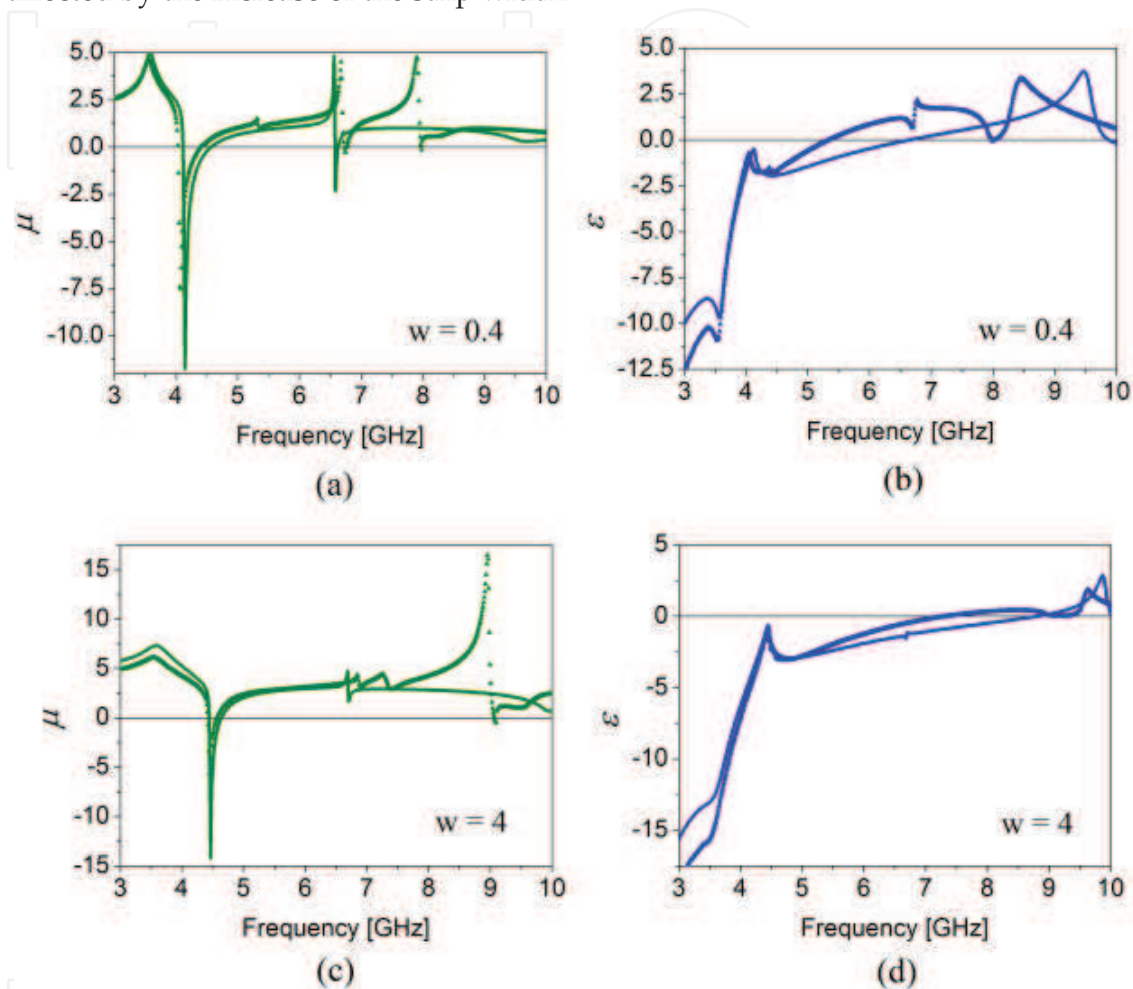


Fig. 13. Frequency dependence of the real parts of the permeability ((a),(c)) and effective permittivity ((b),(d)) for  $w=0.4$  mm and  $w=4$  mm, respectively. Simulation (line) and experimental (symbol) results.

The characteristic frequencies of a Lorentz dispersion law,  $f_o$  and  $f_{pm}$  respectively, remain practically unchanged by the increase of  $w$ . However, a slight frequency shift and narrower window with negative permeability values is observed, which is a consequence of the modified interaction between the SRRs and the wide shunt strip. Derived from these results, wide shunt strips present higher electric plasma frequencies, and consequently deeper rejections in the out-of-band are achieved. More to the point, through this shunt strip enlarging, the coupling between the CPW and the SRRs is reduced, providing narrower bandwidth and higher insertion losses. Both effects are interdependent, and the alteration of  $w$  brings always together a modified rejection in the out-of-band and coupling levels between the SRRs and the line. In both cases the comparison of the measured and calculated

data, shows a relatively good agreement. However, some discrepancy can be noticed. This discrepancy is attributed to different reasons. Two taper sections are used in the fabricated devices, so in order to retrieve effective parameters they have to be de-embedded. This is a possible source of errors. At the same time, finite size ground planes, fabrication tolerances, and the measurement procedure also introduce variations in the experimental response.

### 3.2 Array of split ring resonators loaded coplanar waveguide with wide shunt strips

The previous section has shown that there is a strong relationship between rejection in the out-of-band region, bandwidth, insertion losses, and selectivity as a function of the shunt strip width. Devices with a high selectivity and narrow bandwidth (high  $Q$ ) generally present high values of insertion losses. In contrast, devices with moderate or low insertion losses do not have sufficiently selective responses to accomplish design requirements with restrictive out-of-band rejection or narrow bandwidth. Therefore, the key aspect in narrow band pass filters is the necessity of a trade-off between achievable insertion losses in the pass band and required frequency selectivity. The advantage of using the proposed SRRs loaded CPW line with wide strips is the possibility to fulfill this trade-off, as will be shown, when several unit cells are connected. The topology of the structure and a fabricated prototype are presented in Fig. 14.

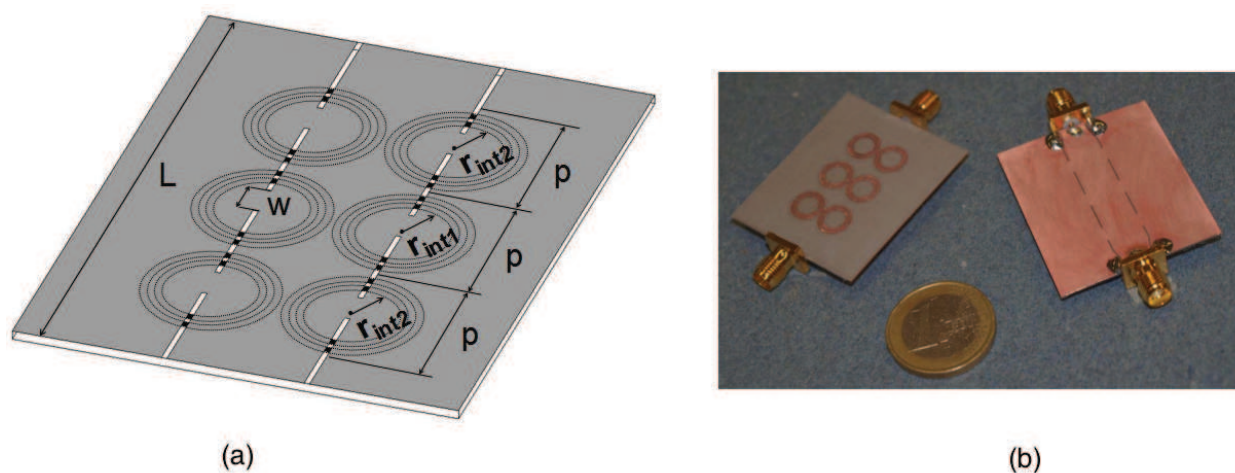


Fig. 14. Model of the SRRs loaded CPW line with wide strips composed of 3 cascaded unit cells.

The proposed structure consists of three optimized stages, where the internal radius  $r_{int1}$  and  $r_{int2}$ , and the unit cell period  $p$  have been modified in order to achieve a reflection coefficient  $S_{11} < -10$  dB along the pass band for two different strip widths  $w=3.5$  mm and  $w=4.5$  mm. After optimization, parameter values used in the process have been set to  $r_{int1}=2.6$  mm,  $r_{int2}=2.58$  mm, and  $p=10$  mm for  $w=3.5$  mm, while  $r_{int1}=2.61$  mm,  $r_{int2}=2.59$  mm, and  $p=9.9$  mm for  $w=4.5$  mm. The total length of the device is  $L=30$  mm. The rest of the cell parameters are the same as those given in Table 1. In Fig. 15 the frequency response of the two optimized filters is shown. In addition, Table 6 summarizes the main properties of the proposed filters. It can be seen that the response of both structures shows excellent insertion loss levels for the two different widths used even if narrow pass bands are achieved. Besides,

good rejections levels, better than -30 dB, below and above the pass band are obtained with small ripple characteristics in the pass band of 0.4 dB and 0.6 dB. The main advantages of the filters proposed are the small insertion losses obtained in very selective filters with compact dimensions. In particular, the advantage of miniaturization when SRRs loaded CPW are implemented can be clearly appreciated in Fig. 16.

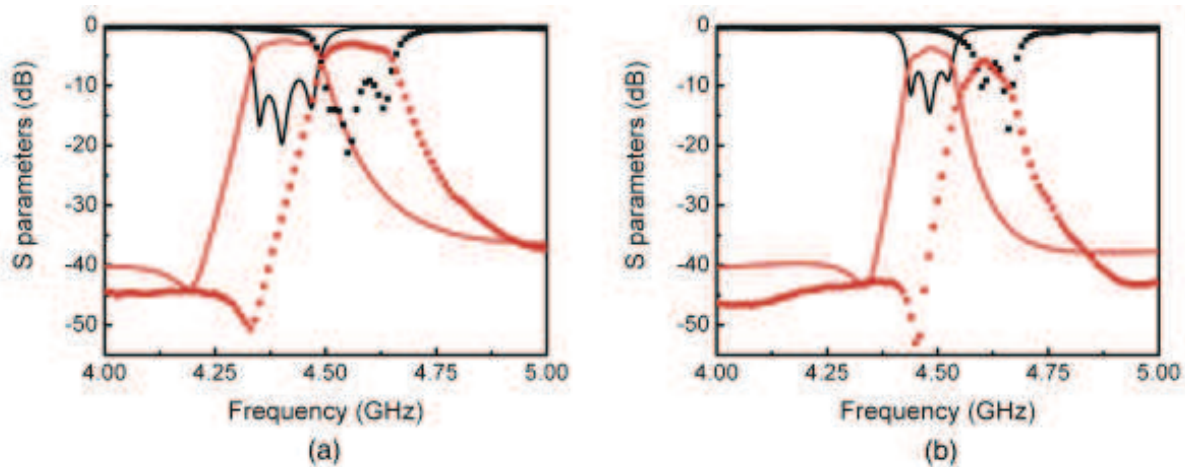


Fig. 15. Simulated (solid line) and experimental (symbol)  $S_{11}$  and  $S_{21}$  parameters for the optimized 3 stage SRRs loaded CPW line with (a)  $w=3.5$  mm, and (b)  $w=4.5$  mm.

	FBW (%)	IL (dB)	Ripple (dB)
$w=3.5$ mm	3.9	1.3	0.4
$w=4.5$ mm	1.8	2.2	0.6

Table 6. Characteristics of the optimized 3 stage SRRs loaded CPW simulated response.

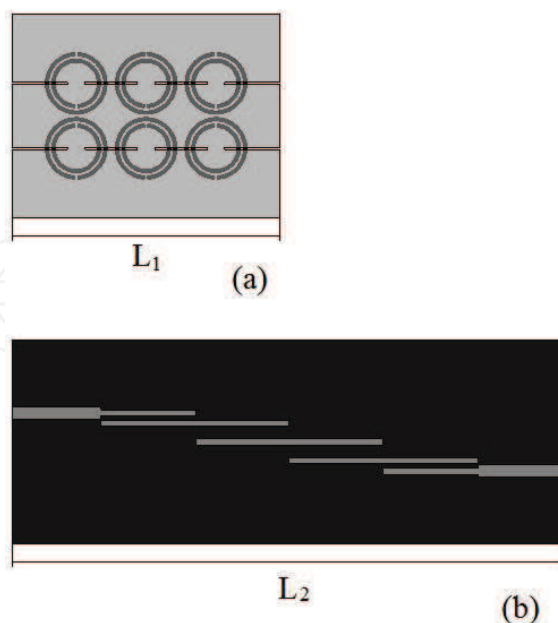


Fig. 16. Comparison of the order-3 layouts. (a) SRRs loaded CPW with wide shunt wires filter, and (b) edge-coupled line filter.

It compares the dimensions of two simulated models, namely the SRRs loaded CPW with wide shunt strips and a conventional edge-coupled lines filter. The total length  $L_1$  is roughly 30 mm (three times the unit cell period), whereas the length  $L_2$  is approximately 68 mm. The proposed filters are shortened by a factor of 2.3. The length of the edge-coupled filter could be further reduced by bending the coupled half-wavelength resonators in a U-shape. However, the order, and thus the length, of the filter cannot be reduced to keep good out-of-band rejection levels. On the contrary, the size of the proposed filter can still be reduced by enlarging the width of the shunt strips. Also, a comparison in terms of S-parameters is shown in Fig. 17. As it can be observed, both filters have a similar behavior. Attenuation levels outside pass band are comparable up to -30 dB for both cases. Also, a slight increment of approximately 1.1 dB in the insertion loss level can be observed for the edge-coupled line filter.

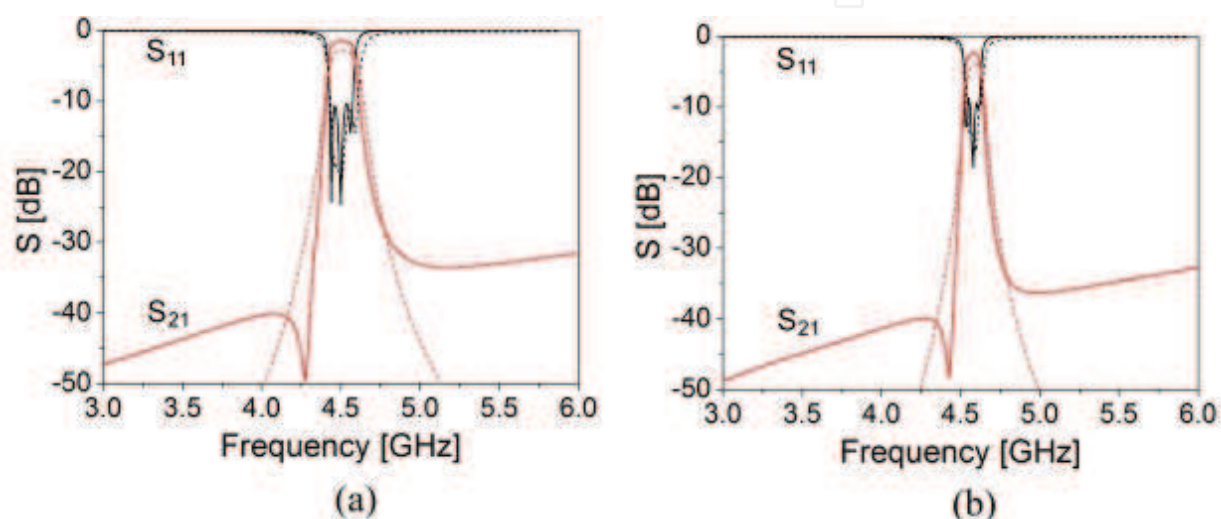


Fig. 17. Simulated  $S_{11}$  and  $S_{21}$  parameters for the optimized 3 stage SRRs loaded CPW line with (a)  $w=3.5$  mm, and (b)  $w=4.5$  mm. Also, the simulated S-parameters for a conventional order-3 edge-coupled filter with similar performance are depicted (dashed line).

#### 4. Synthesis of compact and highly selective filters with tunable responses

This section presents a tunable filter based on the metamaterial transmission lines incorporating dispersive cells. Generally, in order to generate reconfigurable devices, individual reconfigurable components such as tunable capacitors and resonators are used. In particular, this reconfigurable capability is generated by an alteration of the SRRs' resonant frequency using reverse-biased varactors. Subsequently, the adjustable resonant frequency rings are employed to load the host transmission lines.

##### 4.1 Tunable basic cell configuration

Fig. 18 shows the sketch of the varactor diode loaded SRR implemented in a CPW based configuration. The varactor is a reverse-biased semiconductor diode connected between the concentric rings of the SRR. Its capacitance can be tuned by changing the DC voltage applied to its pads. Fig. 19 shows the simulated scattering responses of the basic cell for different values of applied bias voltages (different capacitances and thus SRR resonant frequencies). The tuning range obtained is roughly 1.1 GHz with insertion losses of 2.7 dB for the higher

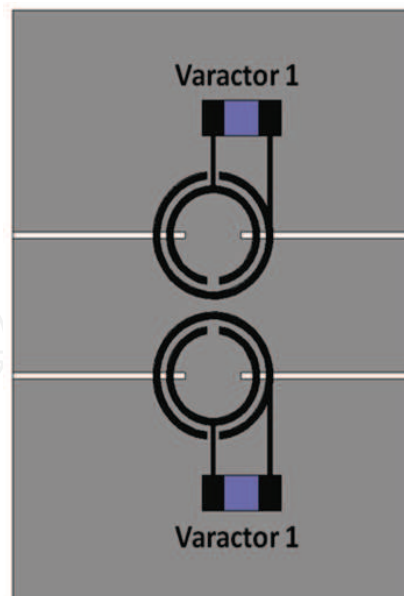


Fig. 18. Basic cell CPW line loaded with wide shunt strips and SRRs based diode varactors. Filter dimensions are the same as in figure 1, except  $w = 4$  mm.

pass band response at around 5 GHz ( $f_{max}$ ), and a maximum value of 3.8 dB when the tunable pass band is shift to 3.9 GHz ( $0.78f_{max}$ ). Moreover, as observed, rejection above the pass band increases as the operating frequency decreases. Compared to other tunable cell configurations, this approach effectively yields a broader frequency tuning range whilst preserving good insertion losses and a very narrow bandpass response.

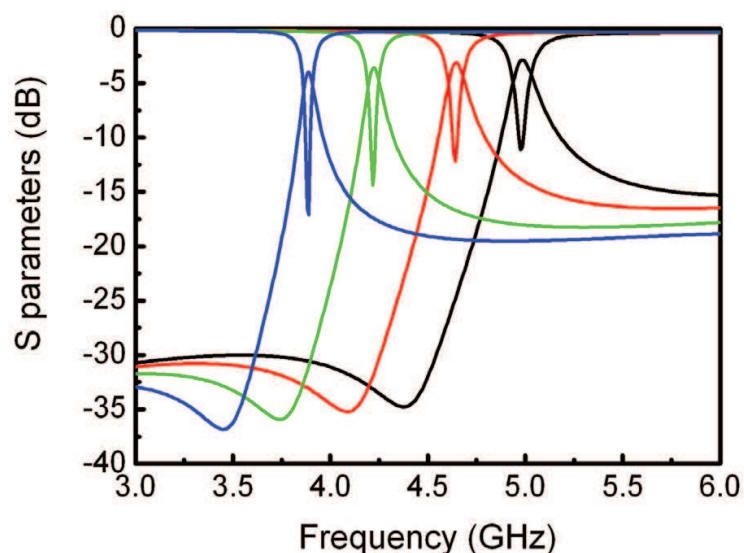


Fig. 19. Simulated scattering parameters of the tunable basic cell.

#### 4.2 Three-cells array of split ring resonators loaded coplanar waveguide with varactors

Next, a synthesis technique for coupled resonators is applied to design a reconfigurable filter. We used the generic coupled resonators scheme of an N-order band pass filter structure by

simply cascading the previous tunable basic cell. A third order reconfigurable band pass filter using varactor loaded SRRs, with a pass band centred between 4 and 5 GHz is considered. The layout of the filter is shown in Fig. 20.

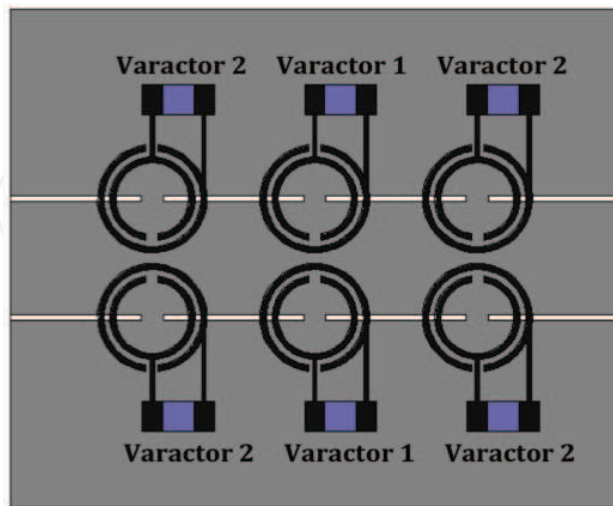


Fig. 20. Three-stage tunable filter loaded with wide shunt strips and diode varactors. Filter dimensions are the same ones as in figure 1, except  $w=2\text{mm}$ .

The design is performed by optimizing independently the central and side stages. In this regard, different loaded SRRs cells are used, with independent diode varactors loading elements as depicted in Fig. 20. The simulated S-parameter results of the third order tunable bandpass filter are shown in Fig. 21. The simulated filter can be tuned from 3.9 GHz to 4.9 GHz (approximately 25% variation), by changing the biasing voltage from 0 to 25 V. The simulated insertion losses at 3.9 GHz are 4.3 dB and 3.2 dB at 4.9 GHz. For the applications where such difference is acceptable, the bandwidth of the filter is calculated to be 2.6% and 5%, respectively.

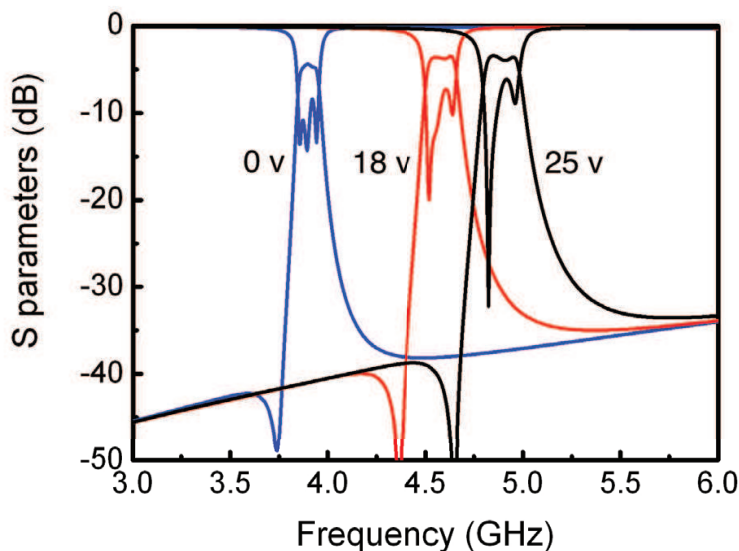


Fig. 21. Optimized simulated response of the 3-stage tunable filter.

Despite the slight increment of the insertion losses in the lower frequency band, the tuning range of the varactor loaded SRR filter is fairly good, and its size is roughly 2.5 times smaller than conventional edge-coupled filters working in the same frequency range. In addition, using a single tunable filter instead of several fixed-frequency filter bands can add system flexibility, which may warrant this slightly augmented insertion losses.

## 5. Summary

In this chapter, different types of coplanar transmission lines loaded with SRRs, shunt wires, series gaps, diode varactors and a combination of them have been analyzed. When different loading elements are added, the left-handed behavior originally predicted for these microstructures can be modified, and their frequency selectivity can be enhanced while maintaining the advantage of miniaturization. The analysis has been performed through full-wave electromagnetic simulations, lumped equivalent circuit models, and measurements of different prototypes.

In section 2, the propagation features of loaded CPW lines have been presented. Left-handed or right-handed propagation can be achieved depending on the loading elements included in the line, using SRRs as a common element. The use of series gaps, and their combination with shunt wires, increases the possibilities of generating narrow transmission bands in the vicinity of the SRR resonance. For instance, they can be tailored to even obtain symmetrical frequency responses. In conclusion, the proposed structures offer an alternative for designing planar frequency filtering structures in applications with severe restrictions in terms of rejection, selectivity, and size.

Section 3 has shown that it is possible to improve the selectivity of highly dispersive transmission lines, made of CPWs loaded with SRRs and shunt wires. This can be achieved by a proper engineering of the electric plasma frequency with respect to the magnetic plasma frequency. Beyond a higher rejection level, which was expected due to the deepening of the forbidden gap between the left- and right-handed dispersion branches, there is also a huge enhancement of the loaded Q quality factors. The structure also maintains low insertion losses. By cascading elementary cells it is possible to achieve a further increase of the steepness of the rejection with low insertion losses. Finally, section 4 has demonstrated reconfigurable filters having narrow bandpass responses, good insertion loss, and good frequency tuning range. The devices were based on varactor diode loaded SRRs and rigorous optimization processes.

Potential use of these miniaturized high-Q frequency selective cells can be foreseen in many modern microwave areas, notably in automotive, radar, wireless communication systems and biosensors.

## 6. References

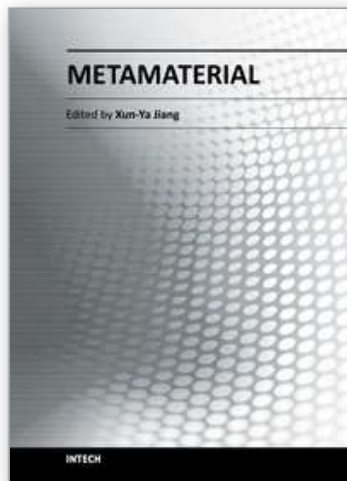
Aznar, F., Bonache, J. & Martin, F. (2008). Improved circuit model for left-handed lines loaded with split ring resonators, *Applied Physics Letters* 92(4): 043512.

- Bonache, J., Martin, F., Falcone, F., Garcia, J., Gil, I., Lopetegui T. and Laso, M. A. G., Marques, R., Medina, F. & Sorolla, M. (2005). Compact coplanar waveguide band-pass filter at the S-band, *Microwave and Optical Technology Letters* 46(1): 33–35.
- Borja, A. L., Carbonell, J., Boria, V. E., Cascon, J. & Lippens, D. (2010). Synthesis of compact and highly selective filters via metamaterial-inspired coplanar waveguide line technologies, *IET Microwaves, Antennas and Propagation* 4(8): 1098–1104.
- Borja, A. L., Carbonell, J., Boria, V. E. & Lippens, D. (2008). Synthesis of compact and highly selective filters via metamaterial-inspired coplanar waveguide line technologies, *Applied Physics Letters* 93: 203505.
- Borja, A. L., Carbonell, J., Boria, V. E. & Lippens, D. (2010a). A 2% bandwidth C-band filter using cascaded split ring resonators, *IEEE Antennas and Wireless Propagation Letters* 9: 256–259.
- Borja, A. L., Carbonell, J., Boria, V. E. & Lippens, D. (2010b). A compact coplanar waveguide metamaterial-inspired line and its use in tunable narrow bandpass filters, *40th European Microwave Conference (EuMC), 26 Sep. - 1 Oct., Paris*.
- Borja, A. L., Carbonell, J., Boria, V. E. & Lippens, D. (2009). Highly selective left-handed transmission line loaded with split ring resonators and wires, *Applied Physics Letters* 94: 143503.
- Carbonell, J., Borja, A. L., Boria, V. E. & Lippens, D. (2009). Duality and superposition in split ring resonator loaded planar transmission, *IEEE Antennas and Wireless Propagation Letters* 8: 886–889.
- Deleniv, A., Vendik, I. & Gevorgian, S. (1999). Modeling gap discontinuity in coplanar waveguide using quasistatic spectral domain method, *2000 John Wiley & Sons, International Journal on RF and Microwave* 10: 150–158.
- Martin, F., Bonache, J., Falcone, F., Sorolla, M. & Marques, R. (2003). Split ring resonator-based left-handed coplanar waveguide, *Applied Physics Letters* 83(22): 4652–4654.
- Mongia, R., Bahl, I. & Bhartia, P. (1999). RF and microwave coupled-line circuits, *Artech House, Boston*.
- Pendry, J. B., Holden, A. J., Robbins, D. J. & Stewart, W. J. (1999). Magnetism from conductors and enhanced nonlinear phenomena, *IEEE Transactions on Microwave Theory and Techniques* 47(11): 2075–2084.
- Pendry, J. B., Holden, A. J., Stewart, W. J. & Youngs, I. (1996). Extremely low frequency plasmons in metallic mesostructures, *Physical Review Letters* 76: 4773–4776.
- Rogla, L. J., Carbonell, J. & Boria, V. E. (2007). Study of equivalent circuits for open-ring and split-ring resonators in coplanar waveguide technology, *IET Microwaves, Antennas and Propagation* 1(1): 170–176.
- Shelby, A., Smith, D. R. & Schultz, S. (2001). Experimental verification of a negative index of refraction, *Science* 292: 7779.
- Shelby, R. A., Smith, D. R., Nemat-Nasser, S. C. & Schultz, S. (2001). Microwave transmission through a two-dimensional, isotropic, left-handed metamaterial, *Applied Physics Letters* 78(4): 489–491.
- Smith, D. R. & Kroll, N. (2000). Negative refractive index in left-handed materials, *Physical Review Letters* 85: 2933–2936.

- Smith, D. R., Padilla, W. J., Vier, D. C., Nemat-Nasser, S. C. & Schultz, S. (2000). Composite medium with simultaneously negative permeability and permittivity, *Physical Review Letters* 84(18): 4184–4187.
- Smith, D. R., Vier, D. C., Koschny, T. & Soukoulis, C. M. (2005). Electromagnetic parameter retrieval from inhomogeneous metamaterials, *Physical Review E* 71(1): 036617.

IntechOpen

IntechOpen



## **Metamaterial**

Edited by Dr. Xun-Ya Jiang

ISBN 978-953-51-0591-6

Hard cover, 620 pages

**Publisher** InTech

**Published online** 16, May, 2012

**Published in print edition** May, 2012

In-depth analysis of the theory, properties and description of the most potential technological applications of metamaterials for the realization of novel devices such as subwavelength lenses, invisibility cloaks, dipole and reflector antennas, high frequency telecommunications, new designs of bandpass filters, absorbers and concentrators of EM waves etc. In order to create a new devices it is necessary to know the main electrodynamical characteristics of metamaterial structures on the basis of which the device is supposed to be created. The electromagnetic wave scattering surfaces built with metamaterials are primarily based on the ability of metamaterials to control the surrounded electromagnetic fields by varying their permeability and permittivity characteristics. The book covers some solutions for microwave wavelength scales as well as exploitation of nanoscale EM wavelength such as visible specter using recent advances of nanotechnology, for instance in the field of nanowires, nanopolymers, carbon nanotubes and graphene. Metamaterial is suitable for scholars from extremely large scientific domain and therefore given to engineers, scientists, graduates and other interested professionals from photonics to nanoscience and from material science to antenna engineering as a comprehensive reference on this artificial materials of tomorrow.

### **How to reference**

In order to correctly reference this scholarly work, feel free to copy and paste the following:

Alejandro L. Borja, James R. Kelly, Angel Belenguer, Joaquin Cascon and Vicente E. Boria (2012). Compact Coplanar Waveguide Metamaterial-Inspired Lines and Its Use in Highly Selective and Tunable Bandpass Filters, *Metamaterial*, Dr. Xun-Ya Jiang (Ed.), ISBN: 978-953-51-0591-6, InTech, Available from: <http://www.intechopen.com/books/metamaterial/compact-coplanar-waveguide-metamaterial-inspired-lines-and-its-use-in-highly-selective-and-tunable-b>

**INTECH**  
open science | open minds

### **InTech Europe**

University Campus STeP Ri  
Slavka Krautzeka 83/A  
51000 Rijeka, Croatia  
Phone: +385 (51) 770 447  
Fax: +385 (51) 686 166  
[www.intechopen.com](http://www.intechopen.com)

### **InTech China**

Unit 405, Office Block, Hotel Equatorial Shanghai  
No.65, Yan An Road (West), Shanghai, 200040, China  
中国上海市延安西路65号上海国际贵都大饭店办公楼405单元  
Phone: +86-21-62489820  
Fax: +86-21-62489821

© 2012 The Author(s). Licensee IntechOpen. This is an open access article distributed under the terms of the [Creative Commons Attribution 3.0 License](#), which permits unrestricted use, distribution, and reproduction in any medium, provided the original work is properly cited.

IntechOpen

IntechOpen